Biochemistry

pubs.acs.org/biochemistry Article

Structural Analyses of Substrate−pH Activity Pairing Observed across Diverse Polysaccharide Lyases

Shubhant Pandey, Bryan W. Berger,* and Rudresh Acharya*

Cite This: https://doi.org/10.1021/acs.biochem.3c00321 Read Online

ACCESS | Metrics & More | Article Recommendations | Supporting Information

ABSTRACT: Anionic polysaccharides found in nature are functionally and structurally diverse, and so are the polysaccharide lyases (PLs) that catalyze their degradation. Atomic superposition of various PL folds according to their cleavable substrate structure confirms the occurrence of structural convergence at PL active sites. This suggests that various PL folds have emerged to cleave a particular class of anionic polysaccharide during the course of evolution. Whereas the structural and mechanistic similarity of PL active site has been highlighted in earlier studies, a detailed understanding regarding functional properties of this catalytic convergence remains an open question, especially the role of extrinsic factors such as pH in the context of substrate binding and catalysis. Our earlier structural and functional work on pH directed multisubstrate specificity of Smlt1473 inspired us to regroup PLs according to substrate type to analyze the pH dependence of their catalytic activity. Interestingly, we find that particular groups of substrates are cleaved in a particular pH range (acidic/neutral/basic) irrespective of PL fold, boosting the idea of functional convergence as well. On the basis of this observation, we set out to define structurally and computationally the key constituents of an active site among PL families. This study delineates the structural determinants of conserved "substrate−pH activity pairing" within and between PL families.

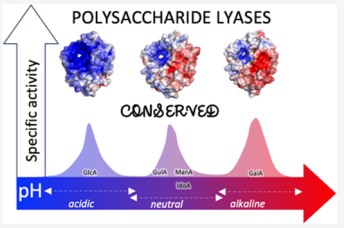

INTRODUCTION

Polysaccharide lyases (PLs) cleave anionic polyuronides in a β-elimination reaction, in which proton abstraction at the C5 position of the uronide ring is followed by cleavage of the ether linkage at the C4 position via a general acid−base catalyst to create an unsaturated product.[1−3] In our previous study, we have elucidated the structural mechanism for a novel pH directed, multifunctional polysaccharide lyase (PL), Smlt1473 (PL-5), from *Stenotrophomonas maltophilia* K279a.[1] It specifically and optimally cleaves poly-hyaluronate, poly-glucuronate, and poly-mannuronate at pH 5.0, 7.0, and 9.0, respectively.[2,3] The unique pH dependence on catalytic activity enabled us to trap bound poly-mannuronate at non-catalytically active pH 5 and 7 in the wild-type Smlt1473 crystal lattice.[1] We furthermore compared the optimum pH for catalytic activity toward a given substrate with that of other monospecific PL families. Like Smlt1473, the PL-8 family of PLs cleaves poly-hyaluronate at acidic pH,[4−6] and PL-5 family of PLs[7−10] cleaves poly-mannuronate at basic pH.[7−9]

Motivated by our prior observations, we divided the PLs on the basis of substrate groups as discussed previously.[11] The substrate grouping is based on the type of substrate that PLs bind at the [+1] subsite and includes (i) galacturonic acid (GalA), (ii) glucuronic/iduronic acid (GlcA/IdoA), and (iii) guluronic/mannuronic acid (GulA/ManA) (Figure 1). In grouping PLs according to substrate type, we have tabulated the information such as substrate group, substrate, PL family and subfamily, E.C. number, source organism, PDB ID, and optimum pH of activity (Table S1). The range of optimum pH for activity for each substrate group establishes the presence of conserved substrate−pH pairing within and among PL families irrespective of variations in structural folds (Figure S1). The structural convergence at the active site as a function of substrate has been reviewed previously.[11] However, these prior studies do not explore the associated functional convergence. Thus, on the basis of our prior studies with Smlt1473, we propose pH as a key, functional convergence factor for analyzing structurally and computationally the PLs selected from each substrate group.

During PL mediated β-elimination, apart from the first charge neutralization step, the next major and pretransition step is C5-H abstraction by a catalytic base from the sugar unit bound at the [+1] subsite.[11] As all the catalytic bases in case of PLs are titratable residues (e.g., His, Tyr, Arg, or Lys), their pK_a value in the substrate-bound state decides the pH value at which these respective bases get activated. Thus, the pK_a value of the residues acting as base defines the base activation pH. At or above this particular pH value, these residues will be in a deprotonated form (His, Arg, and Lys will become neutral by losing their positive charge, and Tyr will develop negative charge) (Figure S2). This is necessary to act as the catalytic base for C5-H abstraction. On the basis of our work and others, it is evident that

Received: June 21, 2023
Revised: August 8, 2023

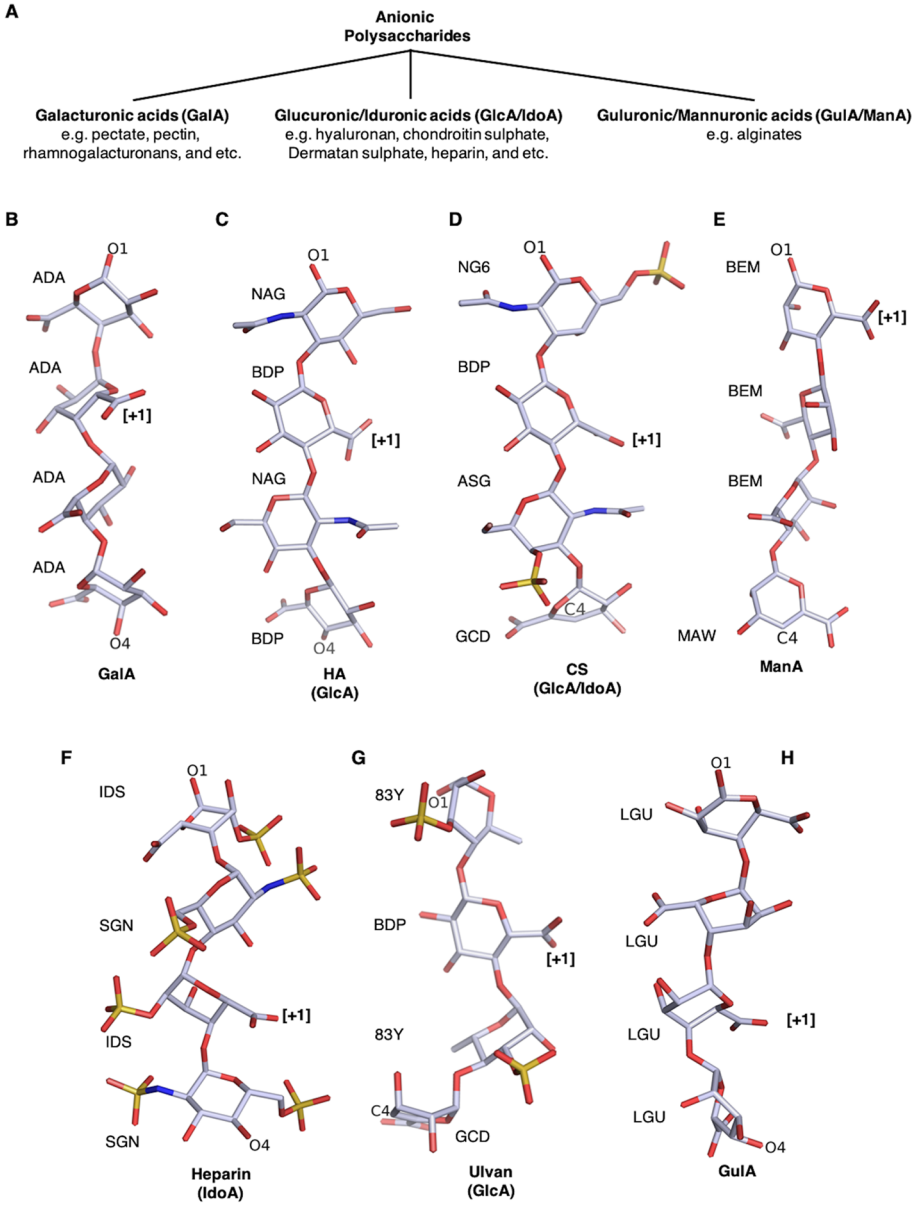

Figure 1. The three main anionic polysaccharide substrate groups are cleaved by PLs. (A) The organization chart depicts the three substrate groups: galacturonic acid (GalA), glucuronic/iduronic acid (GlcA/IdoA), and guluronic/mannuronic acid (GulA/ManA). GalA is modified as pectate, pectin, or rhamnogalacturonan (RG). GlcA and IdoA are C-5 epimer, and similarly are the GulA and ManA. GalA is a major component of pectic substance found in the cell wall of plants, GlcA and IdoA are the major components of glycans found in the extracellular matrix of higher eukaryotes, and GulA and ManA together form alginates, a major component of seaweed such as brown algae; ulvans are GlcAs found in green algae. (B) Poly-GalA (pectate), (C) poly-GlcA (HA = hyaluronic acid), (D) poly-GlcA (CS = chondroitin sulfate), (E) poly-ManA (alginate), (F) poly-IdoA (heparin), (G) poly-GlcA (ulvan), and (H) poly-GulA (alginate). ADA = alpha-D-galactopyranuronic acid, NAG = *N*-acetyl-beta-D-glucosamine, BDP = beta-D-glucopyranuronic acid, NG6 = *N*-acetyl-D-galactosamine 6-sulfate, ASG = *N*-acetyl-4-*O*-sulfo-beta-D-galactosamine, GCD = 4,5-dehydro-D-glucuronic acid, BEM = beta-D-mannopyranuronic acid, MAW = 4-deoxy-D-mannopyranuronic acid, IDS = 2-*O*-sulfo-alpha-L-idopyranuronic acid, SGN = *N*,*O*6-disulfo-glucosamine, 83Y = 6-deoxy-3-*O*-sulfo-alpha-L-mannopyranose, and LGU = alpha-L-gulopyranuronic acid.

the catalytic residues, especially His/Tyr, are involved across the entire pH range of catalytic activity.[1−19]

Therefore, it is important to analyze structurally and computationally the electrostatic microenvironment of the catalytic bases among selected PLs to determine how differences in the microenvironment tune specificity, including both surrounding residues as well as catalytic residues.

If we compare enzymatic activity at different pH values with the idea of an optimum pH observed, the aforementioned base activation pH can be considered as the starting point, and the optimum pH for activity can be considered as the intermediate point of highest activity; outside of this optimum pH, enzymatic activity decreases. In other words, the range of pH values where PLs function is known as the pH range for activity. The PL catalytic surface will lose net positively charged surfaces as the pH increases, decreasing the binding interaction energy between negatively charged substrate and PL. At a certain point, it will become unfavorable, coinciding with the bounds of the "pH range of activity" (Figure S3). However, as prior studies have demonstrated, structurally similar PLs exhibit different functional activities toward substrate and solution conditions, leading to key questions such as the following: (1) what

https://doi.org/10.1021/acs.biochem.3c00321
Biochemistry XXXX, XXX, XXX−XXX

Table 1. PLs Selected for Structural and Computational Analyses

substrate group	substrate	PL name	family	sub family	E.C. no.	organism	PDB ID (apo/ substrate bound)	opt. pH of activity
group I (poly-GalA)	pectate	PelA	PL-1	5	4.2.2.2	*Bacillus* sp. NI6-5	3VMV/3VMW(tri-GalA)	11.5
	pectate	BsPel	PL-1	6	4.2.2.2	*Bacillus subtilis* subsp. *Subtilis* str. 168	1BN8/2O17(hexa-GalA)	8.5
	pectate	PelC	PL-1	3	4.2.2.2	*Dickeya chrrysanthemi* EC16	1O8F/2EWE(penta-GalA)	9.5
	pectate	PL2A	PL-2	1	4.2.2.2	*Yersinia enterocolitica* subsp. *enterocolitica* 8081	2V8J/2V8K(tri-GalA)	9.6
	pectate	PecB	PL-3	1	4.2.2.2	*Caldicellulosiruptor bescii* DSM 6725	3TG9/4Z03(tri-GalA)	8.5
	rhamnogalctouronate	BT4170	PL-9	1	4.2.2.23	*Bacteroides thetaiotaomicron* VPI-5482	5OLQ/5OLS(tri-GalA)	9.0
	pectate	Pel10A	PL-10	1	4.2.2.2	*Cellvibrio japonicus* Ueda 107	1GXM/1GXO(tri-GalA)	10.3
group II (poly-GlcA/IdoA)	hyaluronate	SpnHL	PL-8	1	4.2.2.1	*Streptococcus pnemoniae* R6	1EGU/1LOH(hexa-HA)	6.0
	chondroitin sulfate	CslA	PL-8	3	4.2.2.5	*Pedobacter heprinus* DSM 2366	1CB8/1HMW(tetra-CS)	8.0
	chondroitin sulfate/ hyaluroante	ArthroAC	PL-8		4.2.2.-	*Paenarthrobacter aurescens*	1RWA/1RWF(tri-CS)	6.0 (more activity against HA)
	ulvan	LOR_107	PL-24		4.2.2.-	*Alteromonas* sp. LOR	6BYP/6BYT(tetra-ulvan)	7.5
	heparin	heparinase I	PL-13		4.2.2.7	*Bacteroides thetaiotaomicron* VPI-5482	3IKW/3INA(dodeca-heparin sulfate)	7.5
group III (poly-ManA/GulA)	mannuronate	alginate lyase A1-III	PL-5		4.2.2.3	*Sphingomonas* sp. A1	1QAZ/4F13(tetra-ManA)	8.0
	mannuronate	Smlt1473	PL-5		4.2.2.3	*Stenotrophomonas maltophilia* K279a	7FHX/7FI0(tri-ManA)	9.0
	guluronate	AlyF	PL-6		4.2.2.11	*Vibrio splendidus*	6ITG/6A40(tetra-GulA)	7.5
	guluronate	AlyGC	PL-6	1	4.2.2.11	*Paraglaciecola chathamensis* S18K6T	5GKD/5GKQ(tetra-ManA)	7.0
	guluronate	alginate lyase A1-II	PL-7		4.2.2.-	*Sphingomonas* sp. A1	2CWS/2ZAC(tetra-GulA)	7.5

determines the optimal catalytic pH, (2) does optimal catalytic pH coincide with optimal binding energy for a given substrate, and (3) why do different substrates require different ranges of optimal catalytic pH?

Previously, in an attempt to address these questions, we had calculated the electrostatic surface map of the Smlt1473 wild-type protein structure as a function of pH.[1] We found that at acidic, neutral, and alkaline pH, the respective spread of electropositive surface is maximum, intermediate, and minimum. We anticipate that the change in spread of electrostatic surface as we move across the pH range for activity provides a complementary positive surface to PLs for binding anionic polysaccharides, which is the basis for this current study. Our current work suggests that the optimum pH corresponds to a pH-directed, electropositive surface where binding is optimal. To further clarify the role of pH-directed, charged surfaces in determining the optimum pH range as a function of substrate, we analyzed the positive and negative charged amino acids at active and distal sites across a range of PL families and structures. Specifically, we modeled the Coulombic interaction network based on our pK_a calculations. This allowed us to identify the structural determinants responsible for the observed variation in substrate−pH pairing within and among PL families. We also discuss why certain substrates require specific pH ranges for catalysis. Overall, this study will help to create a foundation for PL structure and design that will inspire the development of future research involving engineering substrate specificity into PLs and other carbohydrate-active enzymes where pH plays a significant functional role in catalysis.

MATERIALS AND METHODS

Selection of PLs for the Structural and Computational Analyses. The PLs tabulated in Table S1 are biochemically and structurally characterized representatives of their family. For this study, we selected PLs that are both enzymatically and structurally characterized in apo as well as substrate-bound form. We had to make sure that the PLs selected for each substrate group cover all possible optimum pH ranges within the substrate-specific pH range of activity. For proper structural and computational analyses, the mutated PL-substrate complex was modeled *in silico* into wild-type by the Rosetta relax protocol. Bad structures, e.g., PDB file containing multiple charge changing mutations, protein sequence from PDB varying significantly from Uniprot sequence, and improperly built ligand and protein structures, were not selected. The PL selected by the above criteria was tabulated (see Table 1).

Rosetta's Fast Relax Protocol. Active site mutations (Arg/His/Lys to Ala/Leu; Tyr to Phe) are generally used to complex the substrate in the crystal structure. For structural analysis and computational pK_a calculation, we mutated the crystal structures *in silico*, which may result in a vdW clash with the substrate. To avoid such a clash, we used Rosetta's fast relax protocol.[20] The usage information, script, and protocol can be found at Rosetta Commons (https://www.rosettacommons.org). It should be

https://doi.org/10.1021/acs.biochem.3c00321
Biochemistry XXXX, XXX, XXX−XXX

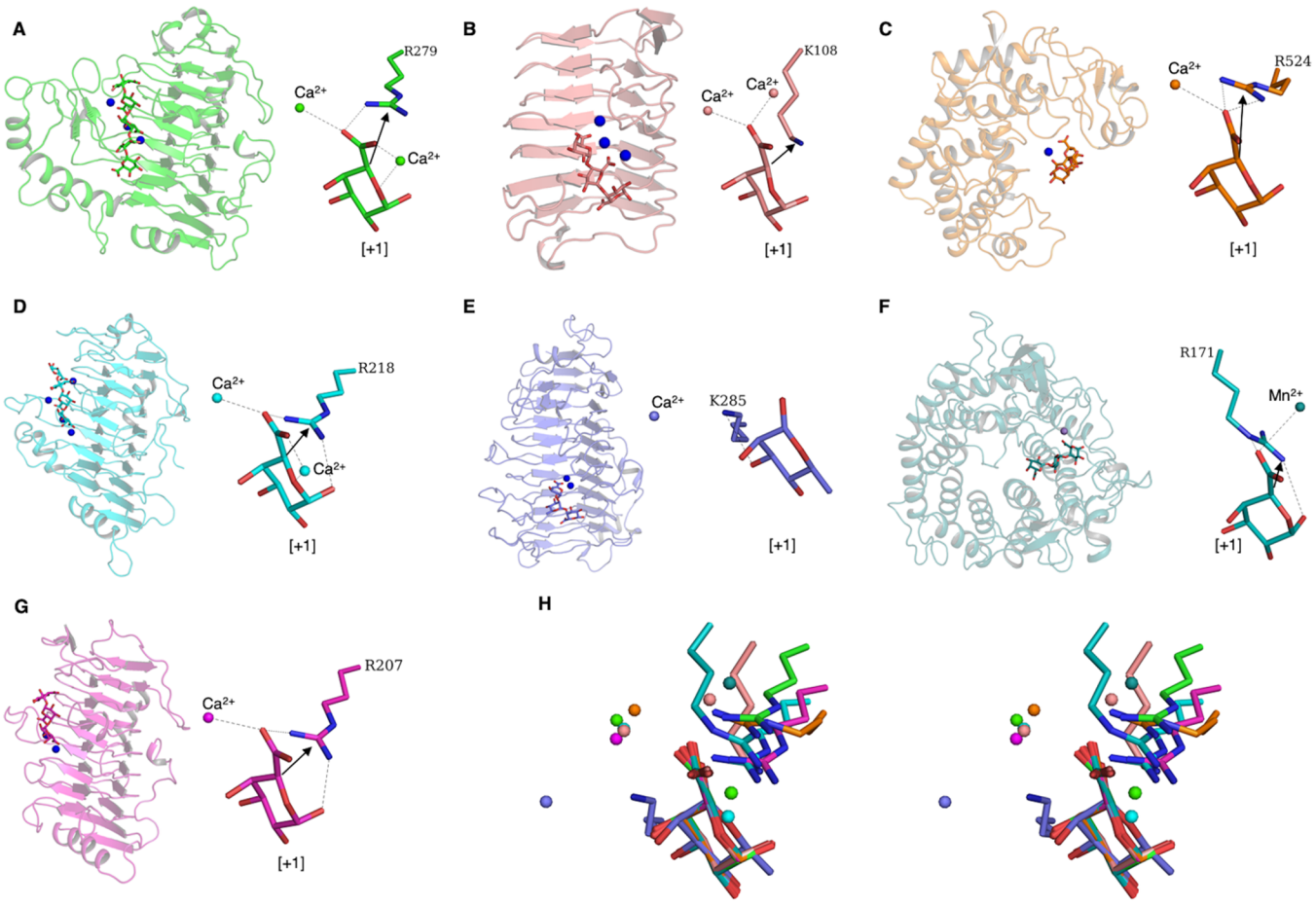

Figure 2. The poly-GalA lyase from various PL families. The cartoon representation of the PL fold and stick representation of the active site at the [+1] subsite of (A) BsPel from *Bacillus subtilis* subsp. *Subtilis* str. 168, PL-1, subfamily-6, PDB ID: 1BN8/2O17; (B) PecB from *Caldicellulosiruptor bescii* DSM 6725, PL-3, subfamily-1, PDB ID: 3T9G/4Z03; (C) Pel10A from *Cellvibrio japonicus* Ueda107, PL-10, subfamily-1, PDB ID: 1GXM/1GXO, (D) PelC from *Dickeya chrysanthemi* EC16, PL-1, subfamily-3, PDB ID: 1O8F/2EWE; (E) BT4170 from *Bacteroides thetaiotaomicron* VPI-5482, PL-9, subfamily-1, PDB ID: 5OLQ/5OLS; (F) PL2A from *Yersinia enterocolitica* subsp. *enterocolitica* 8081 PL-2, subfamily-1, PDB ID: 2V8J/2V8K; and (G) PelA from *Bacillus* sp. N16-5, PL-1, subfamily-5, PDB ID: 3VMV/3VMW. (H) Stereographic image of the superposing substrate (+1 subsite) from all poly-GalA lyases (A−G) for visualizing structural convergence at the active site.

noted that a potential limitation of this approach is one where potential changes in backbone structure are introduced, which may lead to changes in active site configuration. However, to ensure that this is not the case in the current study, we provide in Table S2 a summary of RMSD differences between the wild-type and mutated structures used in this study. Note that in the majority of cases, the RMSD differences are less than 0.2 Å, indicating that no significant changes in the backbone structure occurred.

pK_a Analyses. For both "apo" and ligand-bound structures, we performed pK_a calculations at optimum pH and used the command-line version of PROPKA31 that incorporates ligands and ions into the calculations.[21,22] The result of the pK_a calculation was used to (1) generate H-bond and Coulombic interaction network for the catalytic base and (2) model negative and positive charged amino acid clusters around the active site.

RESULTS AND DISCUSSION

Substrate Dictates the PL Activity as a Function of pH. As all of the amino acids implicated as the catalytic base for PLs are titratable in nature, the pH at which they can act as base is linked to the magnitude of their pK_a values. Thus, amino acids with higher pK_a values act as a base at higher pH and include Arg (pK_a = 12.50), Lys (pK_a = 10.50), or Tyr (pK_a = 10.00); amino acids acting as base at neutral pH include Lys, Tyr, and His (pK_a = 6.50); amino acids acting as base at acidic pH invariably include His. The pK_a values shown in brackets are called model or intrinsic pK_a values calculated by NMR spectroscopy of terminally capped oligopeptide containing one of the above titratable group.[23,24] As described in the Materials and Methods section, we chose to use PROPKA for estimation of pK_a values; this approach offers the ease of rapid calculation but, because of its empirical nature based on primarily near surface residues, can introduce large deviations in calculation for highly buried residues. At solution pH equal to their pK_a values, each amino acid exists in 50% charged and 50% uncharged state. Thus, at pH values below their pK_a value, the amino acids Arg, His, and Lys will remain protonated and carry a net +1 unit (positive charge) and cannot act as base. However, at pH equal to or above their pK_a values, they will be deprotonated and can act as nucleophilic base or proton abstractor. Unlike Arg, His, and Lys, which become neutral after deprotonation at pH above their pK_a value, Tyr becomes negatively charged (Figure S2).

At the catalytic site of PLs, the above discussed intrinsic pK_a values change in response to solvent accessibility, and the electrostatic microenvironment changes drastically in compar-

https://doi.org/10.1021/acs.biochem.3c00321
Biochemistry XXXX, XXX, XXX−XXX

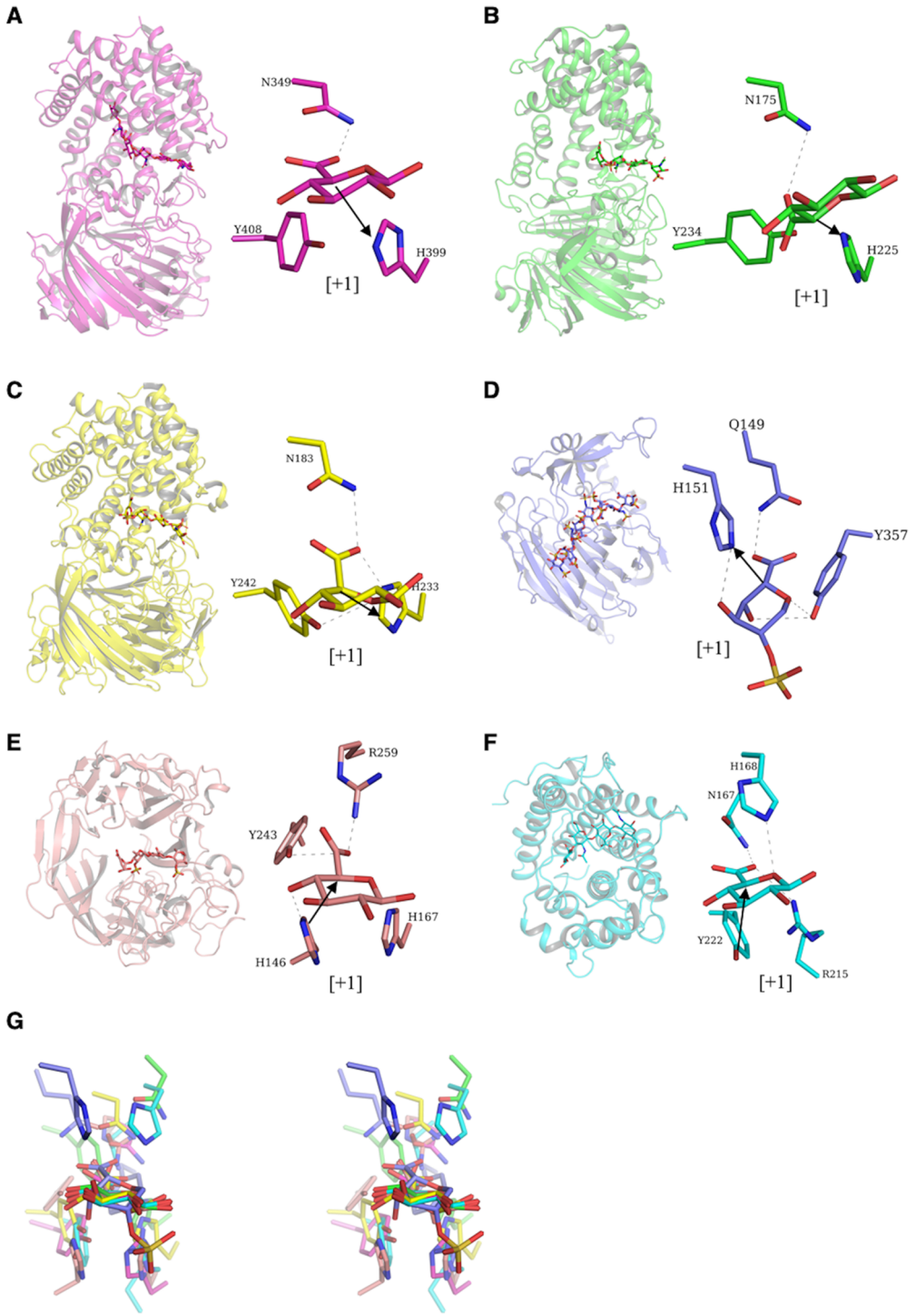

Figure 3. The poly-GlcA/IdoA lyase from various PL families. The cartoon representation of the PL fold and stick representation of the active site at the [+1] subsite of (A) SpnHL from *Streptococcus pneumoniae* R6, PL-8, subfamily-1, PDB ID: 1EGU (apo)/1LOH (hexa-HA); (B) CslA from *Pedobacter heparinus* DSM 2366, PL-8, subfamily-3, PDB ID: 1CB8 (apo)/1HMW (tetra-CS); (C) ArthroAC from *Paenarthrobacter aurescens*, PL-8, PDB ID: 1RWA (apo)/1RWF (iduronated CS); (D) heparinase I from *Bacteroides thetaiotaomicron* VPI-5482, PL-13, PDB ID: 3IKW (apo)/3INA (Heparin); (E) LOR_107 from *Alteromonas* sp. LOR, PL-24, PDB ID: 6BYP (apo)/ 6BYT (ulvan); and (F) Smlt1473 from *Stenotrophomonas maltophilia* K279a, PL-5, PDB ID: 7FHX (apo pH 5)/7FHX (docked HA). (G) Stereographic image of superpose substrate (+1 subsite) from all poly-GlcA/IdoA lyases (A−F) for visualizing structural convergence at the active site.

ison to the fully solvated, small model oligopeptides.[23,24] Moreover, our observation of optimum pH for enzymatic activity for selected PLs belonging to each substrate group is consistent with the above discussion (Table 1, Table S1).

The PLs cleaving group I substrates containing GalA utilize Arg or Lys as the catalytic base. Notably, the observed optimum pH is below the amino acid's respective intrinsic pK_a values. Moreover, among PLs cleaving a particular substrate at a certain range such as alkaline pH, one can find the optimum pH for

https://doi.org/10.1021/acs.biochem.3c00321
Biochemistry XXXX, XXX, XXX−XXX

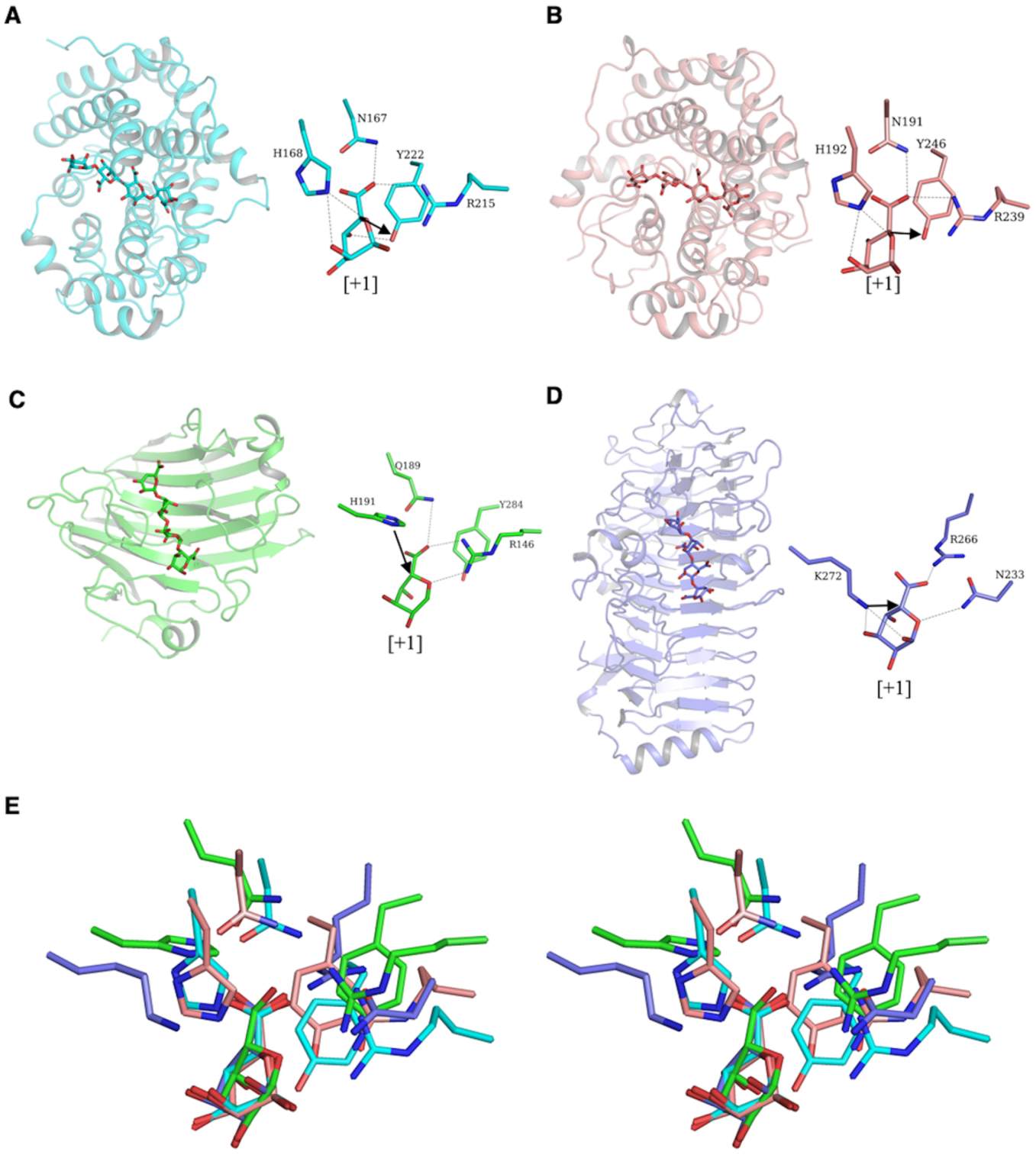

Figure 4. The poly-GulA/ManA lyase from various PL families. The cartoon representation of the PL fold and stick representation of the active site at the [+1] subsite of (A) Smlt1473 from *Stenotrophomonas maltophilia* K279a, PL-5, PDB ID: 7FHZ (apo at pH 9)/7F10 (ManA bound at pH 5.0), 7FI1(ManA at pH -7.0); (B) alginate lyase A1-III from *Sphingomonas* sp. A1, PL-5, PDB ID: 1QAZ (apo)/4F13 (ManA); (C) alginate lyase A1-II from *Sphingomonas* sp. A1, PL-7, PDB ID: 2CWS (apo)/2ZAA (ManA); and (D) AlyF from *Vibrio splendidus*, PL-6, PDB ID: 6ITG (apo), 6A40 (GulA). (E) Stereographic image of superpose substrate (+1 subsite) from all poly-ManA/GulA lyases (A−D) for visualizing structural convergence at active site.

activity at much lower or higher pH values. Specifically, in pectate lyases displaying a parallel β-helix fold, in comparison to the lower range of alkaline optimum pHs for activity of PL-3 family member PecB[25] and PL-9 family member BT4170,[26] the PL-1 pectate lyases PelC[27,28] and PelA[29] show a higher range of alkaline optimum pH values for activity (9.5 and 11.5, respectively). The utilization of lysine as opposed to Arg (PL-1) as catalytic base by PL-3 and PL-9 has been attributed to this

https://doi.org/10.1021/acs.biochem.3c00321
Biochemistry XXXX, XXX, XXX−XXX

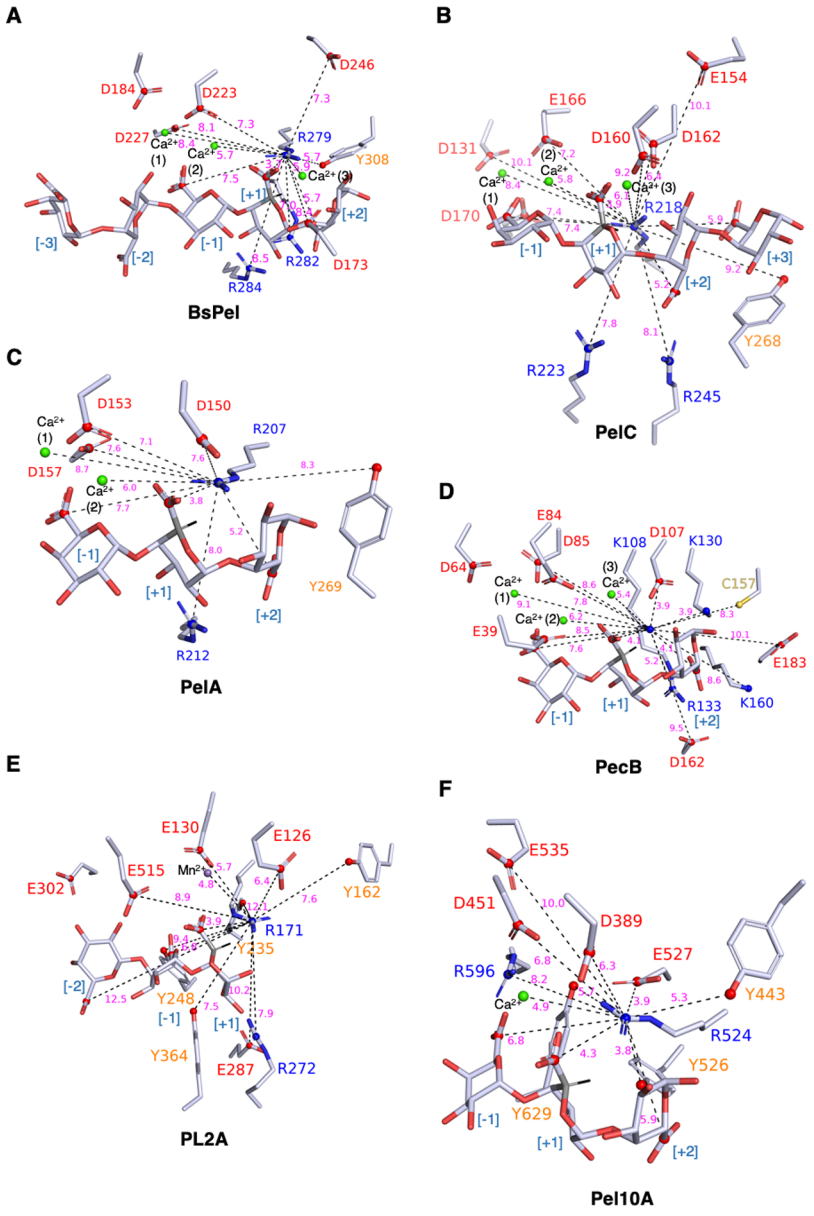

Figure 5. Electrostatic microenvironment around the catalytic base of selected poly-GalA lyases. (A) BsPel complexed with penta-GalA [−3 to +2], three Ca^{2+} ions [−1 to +1], catalytic base: R279 [+1]; (B) PelC complexed with tetra-GalA [−1 to +3], three Ca^{2+} ions [−1 to +1], catalytic base: R218 [+1]; (C) PelA complexed with tri-GalA [−1 to +2], two Ca^{2+} ions [−1], catalytic base: R207; (D) PecB complexed with tri-GalA [−1 to +2], three Ca^{2+} ions [−1 to +1], catalytic base: K108; (E) PL2A complexed with tri-GalA [−2 to +1], Mn^{2+} ion [+1], catalytic base: R171; and (F) Pel10A complexed with tri-GalA [−1 to +2], one Ca^{2+} ion [−1], catalytic base: R524. The Coulombic interactions centered at the catalytic base are shown as dashed lines (black) labeled with distance (magenta). The basic, acidic, and aromatic amino acids constituting the electrostatic microenvironment are represented as a stick model (C = gray, O = red, and N = blue) and respectively labeled with blue, red, and orange colors. The substrates are also shown as the same stick model and labeled with PL's active site surface subsites, negative (left, entry site) to positive (right, exit site). The blue and red nonbonded spheres represent, respectively, the positive charge center of basic amino acids (pK_a lowering) and the negative charge center of the carboxylic group of acidic amino acids and substrates (pK_a raising). The cleavable glycosidic oxygen lies in between the [−1, +1] subsite; the catalytically important substrate's C5 atom at the [+1] subsite is shown in gray color with bonded labile H atom represented as a black line.

observed difference in pH maximum for activity.[25] In particular, the low pK_a of Lys will lead to its deprotonation at lower pH to act as base, hence the low pH observed for activity.[25] However, despite this general trend, we note that BsPel (PL-1) has a lower optimum pH of 8.5 as PL-3 and PL-9 but still uses Arg as the catalytic base.[30] This observation further validates that the microenvironment of the catalytic base is more important than the choice of catalytic base itself in deciding the optimal pH for activity. The other GalA lyase from family PL-2[31] and PL-10,[32] which display structurally dissimilar $(\alpha/\alpha)_n$ barrel folds, also utilizes Arg as the catalytic base and, like the aforementioned parallel β-helix GalA lyase, utilizes metal ion for substrate binding. It also has optimum pH for activity in a higher alkaline range as do PelA and PelC. Figure 2 depicts the proteins selected in group I.

Among PLs cleaving group II substrates (GlcA/IdoA), the PL-8 family of PLs displaying $(\alpha/\alpha)_n$ barrel and anti-parallel β-sheets cleaves hyaluronic acid at acidic pH (SpnHL, ArthroAC, ScPL8Hyal) but cleaves chondroitin sulfate (CslA) at alkaline pH. Like PL-5 enzymes, the PL-8 family of PLs is known to

https://doi.org/10.1021/acs.biochem.3c00321
Biochemistry XXXX, XXX, XXX−XXX

utilize His and Tyr as catalytic base and acid, respectively.[4−6,12−14] However, the only difference is that PL-8 His and Tyr are in *syn* position compared to *anti* of PL-5. Interestingly, another chondroitin sulfate lyase from family PL-6, which displays parallel β-helix like pectate lyase, uses metal ions for substrate binding and Arg as catalytic base and thus utilizes alkaline pH for enzymatic activity[15,16] (Table 1, Table S1). The heparin lyase heparinase-I (PL-24) cleaves the most negatively charged anionic polysaccharide heparin sulfate near neutral pH of 7.5.[17] It displays β-jellyroll fold and utilizes the His/Tyr system similar to Smlt1473. The last selected PL from this group includes ulvan lyase LOR_107 (PL-13), cleaves sulfated GlcA substrate at pH 7.5, and displays a less characterized β-propeller fold. It also contains a structurally similar His/Tyr system as PL-8 enzymes, but His has been implicated to act as both acid and base[18] (Figure 3).

Among PLs cleaving group III substrates (ManA/GulA), the PLs selected for ManA include only well characterized PL-5 enzymes, whereas for GulA, we have included PL-6 and PL-7 enzymes. The PL-5 family member Smlt1473, alginate lyase A1-III [$(\alpha/\alpha)_n$ barrel] and PL-7 alginate lyase A1-II (β-sandwich) are structurally diverse but have a similar His/Tyr catalytic system.[1,7−9,19] The PL-6 AlyF displays a parallel β-helix as pectate lyase and similarly utilizes Arg as the catalytic base but does not use metal ions for ligand binding.[33] The optimum pH for ManA lyase is in the alkaline pH range, and in spite of structural divergence, PL-6 (parallel β-helix) and PL-7 (β-sandwich) utilize the optimum pH of 7.5 (Figure 4).

We found from the above structural analysis that the PLs with parallel β-helix fold cleave substrates from each group such as pectate (GalA), chondroitin sulfate (GlcA/IdoA), and poly-GulA (GulA/ManA) but retain the Lys/Arg catalytic system. Except for AlyF (poly-GulA lyase, optimum pH = 7.5), they utilize metal ions for substrate binding and charge neutralization and maintain an alkaline range of pH for optimal activity. On the other hand, the PLs displaying $(\alpha/\alpha)_n$ barrel fold utilize a different catalytic mechanism for GalA (Lys/Arg system, metal ion, alkaline pH for optimal activity) in comparison to GlcA/IdoA and GulA/ManA (His/Tyr system, substrate specific pH for optimal activity).

Therefore, we observed that PLs displaying $(\alpha/\alpha)_n$ barrel fold show high divergence at the active site and thus maintain various ranges of substrate-specific optimum pH values (Table 1). This is in contrast to PLs displaying parallel β-helix folds, which show high convergence at the active site but still maintain various substrate-specific optimum pH values (Table 1) by subtle arrangements of flanking residues. The other selected PLs, which contain folds such as β-propeller (LOR_107, a PL23 ulvan lyase), β-sandwich (alginate lyase A1-II, a PL-7 poly-GulA lyse), or β-jellyroll (heparinase-I, a PL-13 heparin sulfate lyase), utilize a His/Tyr system and show neutral and near-neutral range of optimum pH for activity. Finally, we conclude that structural convergence may not entirely coincide with pH dependent activity-based functional convergence. In contrast, we find that, irrespective of convergence and divergence in their fold and catalytic geometry, the PLs have evolved to structurally and mechanistically adjust themselves to maintain a strict substrate−pH pairing. The pK_a of PL's catalytic base is determined by the electrostatic interactions available at the active site after substrate binding. To understand what affects the pK_a values of PL catalytic base residues, we have performed structural modeling and computational pK_a analyses of selected PLs (see Materials and Methods). A brief primer on general theories (Born effect, H-bonding, Coulombic interactions) regarding pK_a perturbation is detailed in the Supporting Information (Note S1).

PLs Binding GalA at the [+1] Subsite Displaying Parallel β-Helix Fold. The most common feature among these PLs is the presence of metal ions (Ca^{2+} and Mn^{2+}) mainly at the [−1, +1, +2] subsite (Figures 2 and 5). Metal ions most often play a critical role in substrate binding, positioning, and charge neutralization step of the β-elimination reaction mechanism. The other common feature of these PLs is utilization of basic amino acids Arg or Lys as the catalytic base and utilization of alkaline pH for catalytic turnover.[25−32]

The in-depth structural description of fold architectures among these PLs is provided in the Supporting Information (Figure S4A,B). As discussed previously, the PLs cleaving GalA containing substrates occupy different optimum pH positions in the alkaline pH range. The PLs (PL-3 and PL-9) occupying a lower alkaline pH range (8−9) generally use Lys as catalytic base, and PLs (PL-1, PL-2, PL-10) occupying a higher alkaline pH range (9.5−11.5) use Arg as catalytic base.[25] However, in our analysis, we found a poly-GalA lyase, BsPel, which utilizes Arg as catalytic base and utilizes a lower alkaline pH range of optimum activity (8.5) as PL-3 and PL-9.[30] Thus, the PL-1 family of pectate lyases provides a first opportunity to discern the mechanism of the wide optimum pH variation (8.5−11.5) within a PL family. We performed sequence and structural comparisons and identified some key similarity and differences. PelA (subfamily-5) has minimal T3 insertion followed by PelC (subfamily-3), whereas BsPel (subfamily-6) has significant T3 insertion (Figure S4D,E,H,I). The structural alignment in terms of RMSD has the following order: [PelC-PelA] > [BsPel-PelA] > [PelC-BsPel]. PelA being intermediate subfamily-5 superimposes well with both PelC and BsPel, but there is significant RMSD between PelC and BsPel (Figure S4C−S4E). A similar trend is followed for substrate-bound structures as well (Figure S4G−I); however, removal of T3 insertion from both PelC and BsPel results in significantly improved RMSD (Figure S4F). Our further analyses of active site constituent amino acids among these PLs reveal the role of T3 insertion in shaping the electrostatic microenvironment by adding Ca^{2+} binding amino acid residues. In contrast to PelA, the T3 insertion contributes a pair of amino acids for both PelC (D160, D162) and BsPel (D173, N180) that help them bind Ca^{2+} ion at the [+1] subsite (Figure S5D,E).

In the case of BsPel, the catalytic base R279 in the apo state face pK_a lowering determinants that include positive Coulombic interactions from a bound Ca^{2+} ion and R284 at the [+1] subsite. The determinants of increased pK_a include negative Coulombic interactions from D184, D223, and D227 at the [−1] subsite and D173, D246, and Y308 at the [+2] subsite (Table S3). The BsPel in the substrate-bound state coordinates two more calcium ions at the [−1] subsite; the pK_a-lowering determinant R284 and Ca^{2+} ions are the same as the apo state. The pK_a raising determinants apart from D173, D223, D227, D246, and Y308 include additional negative Coulombic interaction from the substrate carboxylic groups at the [−1, +1, +2] subsites. The negatively charged residue D184 does not interact with R279 in the substrate bound state, as it is shielded by two extra Ca^{2+} ions binding at the [−1] subsite (Table S3, Figure 5A).

Similar to BsPel, the PelC catalytic base R218 at the [+1] subsite in apo state also faces one Ca^{2+} ion and a basic amino acid R245 at the [+1] subsite. The pK_a increasing determinants include D131, E166, and D170 at the [−1] subsite; D162 at the

https://doi.org/10.1021/acs.biochem.3c00321
Biochemistry XXXX, XXX, XXX−XXX

[+2] subsite; and Y268 at the [+3] subsite. In the bound state, the pK_a increasing determinants include two additional bound Ca^{2+} ions at the [−1] subsite and R245 (Table S3). In contrast to BsPel, the PelC in the bound state interacts with extra negatively charged residues apart from D131, D162, E166, D170, and Y268. The additional negatively charged residues include E154 and D160 at the [+2] subsite. Moreover, there are a greater number of substrate-interacting carboxylic groups for PelC at the [−1, +1, +2, +3] subsite in comparison to BsPel (Table S3, Figure 5B).

As discussed above, the PelA catalytic base R207 at the [+1] subsite in apo state does not have a conserved Ca^{2+} binding site (Figure S5A−C). The only pK_a lowering residue is R212, whereas pK_a increasing determinants include D153 and D157 at the [−1] subsite, D150 at the [+1] subsite, and Y269 at the [+3] subsite (Table S3). In the bound state, the pK_a increasing determinants include two Ca^{2+} ions and residue R212. The pK_a raising determinants include the same amino acid residues as the apo state, namely, D153, D157, D150, and Y269. The contributions from bound substrate include carboxylic groups from the [−1, +1, +2] subsite (Table S3, Figure 5C). However, we can anticipate more electronegative contribution from the substrate occupied at other positive subsites (not modeled in the relaxed structure) as in the original PDB deposited structure where the co-crystallized product is complexed without Ca^{2+} ion, the substrate occupies [+2, +3, +4] subsites.[29]

From the above results, it is clear that the structural differences (Figure S4A,B) at the active site due to sequence insertion can lead to considerable changes that affect the substrate binding property of the active site within the same family of PL. We observed that Ca^{2+} ions are mainly bound at the [−1, +1] subsite in all selected PL-1 family members of PLs. In case of BsPel, they are able to shield the significant negative charge contribution from the acidic amino acids and substrate carboxylic group from negative subsites [−]. In contrast, PelA and PelC, where substrates mostly occupy [+] subsites, the bound Ca^{2+} ions are not able to shield the negatively charged contribution to the catalytic base. Moreover, like BsPel and PelC, the PelA does not bound Ca^{2+} ion at the [+1] subsite, which further led to the increase in negative charge contribution to its catalytic base. Thus, it is evident why PelA has a higher position in the alkaline range of activity followed by PelC and BsPel based on structural differences at the active site due to sequence insertion and Ca^{2+} ion binding.

The other family of pectate lyases that show a parallel β-helix includes family PL-3 (PecB) and PL-9 (BT4170), which as discussed above utilize the Lys residue as catalytic base whose solution pK_a is usually lower than that of Arg. The PecB in apo state binds Ca^{2+} ion at the [+1] subsite; the other pK_a lowering determinants for catalytic base K108 include R133 at the [+2] subsite and K130 and K160 at the [+3] subsite. The pK_a raising determinants include E39, D64, E84, and D85 at the [−1] subsite and D107 at the [+2] subsite (Table S4). In the bound state, the PecB binds two more Ca^{2+} ions at the [−1] subsite and retains the same basic residues as pK_a lowering determinants R133, K130, and K160. Although the number of pK_a raising determinants has increased, apart from E39, E84, D85, and D107, the new contributors include residues at and toward the [+3] subsite: C157, D162, and E183. The residue D64 does not contribute in the bound state as the Ca^{2+} ion at the [−1] subsite shields the possible interaction (Table S4, Figure 5D); a similar occurrence has been explained above in the case of BsPel (Figure 5A). However, the increase in the number of negative charge interactions upon substrate binding is similar to that of PelC. Interestingly, in both cases, these negatively charged substrates are at [+] subsites, indicating their possible role in product release. The other PecB pK_a raising contribution comes from all carboxylic groups of bound substrates at [−1, +1, +2] subsites. As we do not have a GalA substrate modeled in case of the BT4170 structure at the [+1] subsite, we have not performed in-depth structural and computational work for comparative analyses.

PLs Binding GalA at the [+1] Subsite Displaying $(\alpha/\alpha)_n$ Barrel Fold. The last structurally and biochemically characterized poly-GalA lyases selected for analyses include the PLs of family PL-2 (PL2A) and PL-10 (Pel10A), which display $(\alpha/\alpha)_n$ barrel fold. Like PL-1, they (PL2A and Pel10A) utilize Arg as the catalytic base, possess a high optimum pH for activity, and depend upon divalent cations for their catalytic activity. The Pel10A, like PL-1 pectate lyase, utilizes Ca^{2+} ion, whereas PL2A utilizes Mn^{2+} ion for charge neutralization. The Pel10A in apo state has one Ca^{2+} ion at the [−1] subsite as a pK_a lowering determinant. In contrast, the pK_a raising determinants for catalytic base R524 include H-bond interaction from E527 and Y629 at the [+1] and [−1] subsite, respectively. The pK_a raising determinants involved in electrostatic interactions include D389, E527, and Y526 at the [+1] subsite; D451 and Y629 at the [−1] subsite; and Y443 at the [+2] subsite (Table S4). In the bound state, apart from Ca^{2+} ion, R596 at the [−1] subsite is another pK_a lowering determinant. The pK_a raising determinants are the same as the apo state: D389, E527, Y526, D451, Y629, and Y443. However, the substrate binding results in one more pK_a raising Coulombic interaction from E535 oriented toward the [−1] subsite (Table S4, Figure 5F).

The PL2A catalytic base R171 in the apo state has only bound Mn^{2+} ion as pK_a lowering determinant; the pK_a raising determinants include E302 toward the [−2] subsite; E515, Y235, Y248, and Y364 at the [−1] subsite; and E130 at the [+1] subsite. In the substrate bound state, Mn^{2+} is along with R272 at the [+1] subsite as a pK_a lowering determinant. The pK_a raising determinants apart from E130, E515, Y248, and Y364 include a new contribution from E287 at the [+1] subsite and E126 and Y162 at the [+2] subsite (Table S4). In the bound state, E302 and Y235 do not contribute in raising catalytic base pK_a because the rotameric transition of catalytic base toward the [+] subsite precludes Coulombic interaction from [−] subsites after substrate binding. Similarly, the rotameric transition leads to the gain of new interactions toward [+] subsites: E126, E287, and Y162. The carboxylic groups from [−1, +1] subsites are other contributors in raising catalytic base pK_a (Table S4, Figure 5E).

The major difference observed between the poly-GalA lyase of two fundamentally different folds is that PLs displaying parallel β-helix fold coordinate additional metal ions toward [−] subsites after substrate binding compared to PLs displaying $(\alpha/\alpha)_n$ barrel fold, which in apo as well as bound states bind only one metal ion at the [−1 or + 1] subsite. The other major difference is the composition of amino acids at the active site; the PLs displaying parallel β-helix fold have more Asp (D) and less Glu (E) residues as pK_a raising determinants. In contrast, the PLs displaying $(\alpha/\alpha)_n$ barrel fold has mainly Glu (E) and Tyr (Y) residue as pK_a raising determinants. The presence of more Tyr residue is one of the characteristics of the $(\alpha/\alpha)_n$ barrel fold, which is apparent in our subsequent analysis of the poly-GlcA/IdoA and poly-ManA lyase detailed below.

https://doi.org/10.1021/acs.biochem.3c00321
Biochemistry XXXX, XXX, XXX−XXX

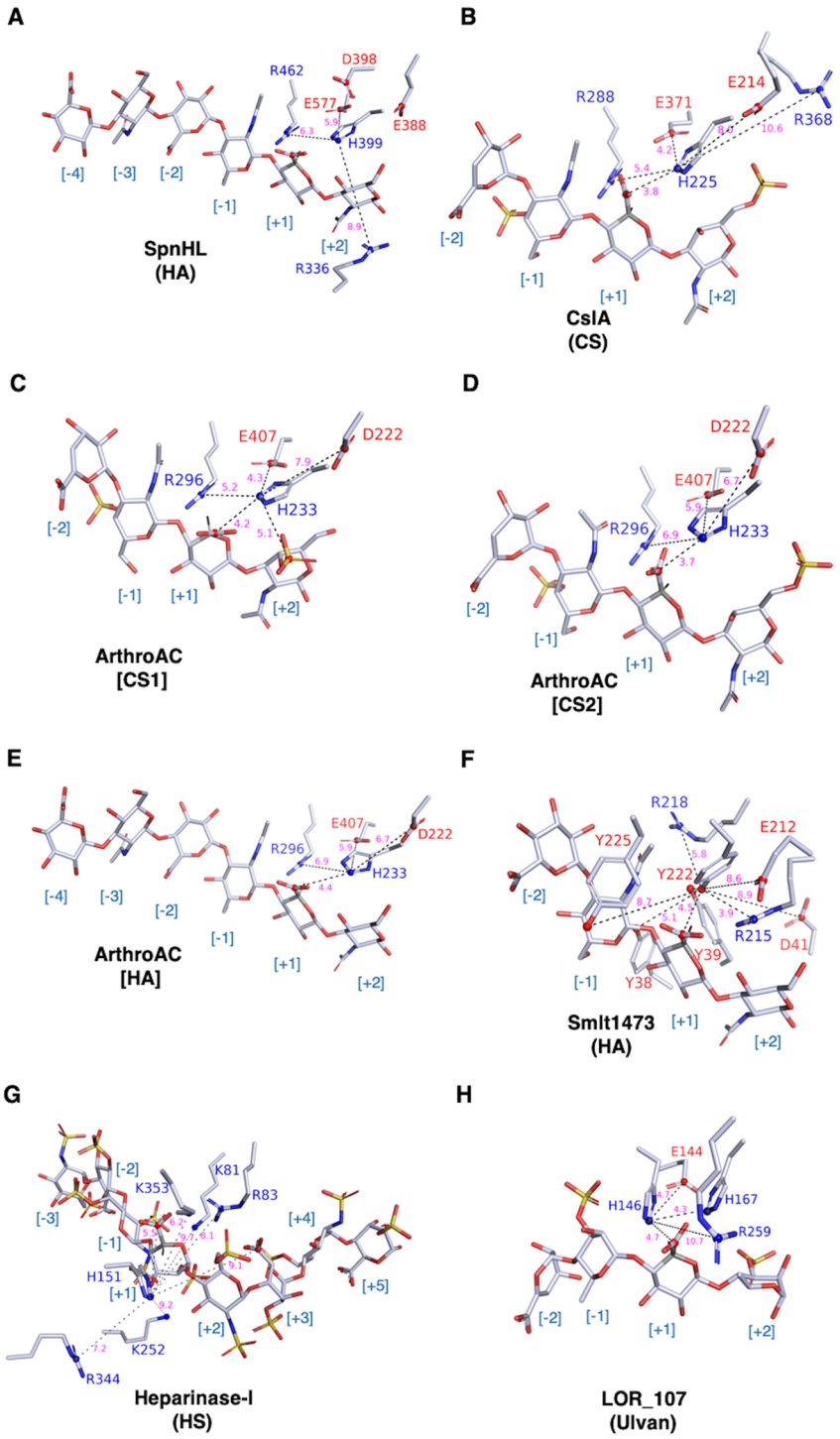

Figure 6. Electrostatic microenvironment around catalytic base of selected Poly-GlcA/IdoA lyases. (A) SpnHL complexed with hexa-HA [−4 to +2], catalytic base: H399 [+1]; (B) CslA complexed with tetra-CS [−2 to +2], catalytic base: H225 [+1]; (C) ArthroAC complexed with tetra-CS1 [−2 to +2]; CS1 has a sulfate group at the C4 position of CS substrate at the [+2] subsite, catalytic base: H233; (D) ArthroAC complexed (modeled) with tetra-CS2 [−2 to +2]; CS2 has a sulfate group at the C5 position of CS substrate at the [+2] subsite, catalytic base: H233; (E) ArthroAC complexed (modeled) with hexa-HA [−2 to +2], catalytic base: R171; (F) Smlt1473 complexed (modeled) with tetra-HA [−2 to +2], catalytic base: Y222; (G) heparinase-I complexed with octa-HS [−3 to +5], catalytic base: H151; and (H) LOR_107 complexed with tetra-Ulvan [−2 to +2], catalytic base: H146. The figure coloring and styling are the same as Figure 5 (see figure legends).

PLs Binding GlcA at the [+1] Subsite Displaying $(\alpha/\alpha)_n$ *Barrel + Antiparallel β-Sheet Fold.* The poly-GlcAs such as hyaluronic acid (HA), chondroitin sulfate (CS), and ulvans are structurally variable because of their polymeric structure and also because of various degrees of substitution replacing sugar hydroxyl groups. These substitutions provide each class of sugar distinct chemical properties such as varying negative charge densities. As discussed earlier, the aforementioned sugars not only differ in their structures but also have a very specific range of pH values where PLs will cleave. HA invariably is cleaved at

https://doi.org/10.1021/acs.biochem.3c00321
Biochemistry XXXX, XXX, XXX−XXX

acidic pH, CS based on its composition can have either acidic or alkaline optimum pH, and ulvan is cleaved at near-neutral pH. First, we will discuss the PL-8 family of poly-GlcA lyase, where we have chosen an HA specific lyase (SpnHL, opt. pH = 6.0), CS specific lyase (CslA, opt. pH = 8.0), and bifunctional lyase that cleaves both HA and CS (ArthroAC, optimum pH 6.0, more active against HA).

SpnHL in apo state has two pK_a lowering determinants for catalytic base H399 at the [+1] subsite: R462 at the [+1] subsite and R336 at the [+2] subsite. The pK_a raising determinants include H-bond interaction and Coulombic interaction from E577 at the [+1] subsite. The other such Coulombic interaction is contributed from D398 at the [+1] subsite and E388 at the [+2] subsite (Table S5). In the HA bound state, the pK_a lowering determinants are the same as the apo state: R336 and R462. However, the pK_a raising determinants include H-bond interaction with sugar ring oxygen atom at the [+1] subsite and single Coulombic interaction from E577 (Table S5, Figure 6A).

In contrast to SpnHL, the CslA in apo state has only one pK_a lowering determinant, R288, at the [+1] subsite for catalytic base H225. The pK_a raising determinants include H-bond and Coulombic interactions from E371 at the [+1] subsite and the other Coulombic interaction from E214 at the [+2] subsite (Table S5). In the bound state, the catalytic base pK_a lowering determinants apart from R288 include R368 at the [+2] subsite. The pK_a raising determinants include H-bond interaction with sugar ring oxygen atom and E371 at the [+1] subsite, Coulombic interaction from E371 via the carboxylic group at the [+1] subsite, and E214 at the [+2] subsite. It is evident from the analysis of pK_a that CslA catalytic base H225 experiences more negative charge interaction for both apo and bound states in comparison to SpnHL catalytic base H399. Thus, CS specific CslA has a higher optimum pH than HA specific SpnHL (Table S5, Figure 6B).

Like CslA, the ArthroAC's catalytic base H233 in apo state faces only one pK_a lowering determinant: R296 at the [−1, +1] subsite. The pK_a raising determinants include the main chain H-bond contribution from H233 itself and Coulombic interaction from D222 and E407 at the [+1] subsite (Table S5). In the CS bound state (ArthroAC [CS1]), the pK_a lowering determinant is the same as the apo state: R296. Similarly, the pK_a raising determinants from apo state are maintained: D222 and E407. However, the position of the catalytic base in between carboxylic groups at the [+1] subsite and sulfate group at the [+2] subsite leads to pK_a raising interactions that include H-bonds (i) from sugar ring oxygen atom and carboxylic group at the [+1] subsite and (ii) two H-bond interactions from the sulfate group at the [+2] subsite (Table S5, Figure 6C). This particular CS substrate raises the pK_a of ArthroAC in the alkaline pH range, which is much higher than its acidic optimum pH reported in the literature. Thus, we modeled a CS substrate (CsIA) with varying positions of the sulfate group and relaxed the modeled structure (ArthroAC [CS2]) to recalculate the pK_a. With new calculations, the pK_a lowering determinant is the same as before: R296; apart from the usual pK_a raising Coulombic interaction from D222 and E407, the other pK_a raising determinants include two H-bond interactions from carboxylic group oxygen at the [+1] subsite (Table S5, Figure 6D). The pK_a raising contribution of the sulfate group at the [+2] subsite is not possible because of its differed position on the sugar ring as compared to the original bound substrate. Thus, the catalytic base pK_a of this structural model is consistent with the observed acidic range of optimum pH. Moreover, the orientation of carboxylic groups is also not in an ideal position for titration to form Coulombic interactions in the bound state. This result shows that a slight variation in substrate structure can have a drastic effect on determining the resulting catalytic pK_a base. Finally, we modeled an HA substrate from SpnHL into ArthroAC coordinates, relaxed the model (ArthroAC [HA]), and subjected it to pK_a calculation. In the HA bound state, the pK_a lowering determinant at the [+1] subsite is the same as others: R296. The pK_a raising determinants include D222, E407, and the carboxylic group at the [+1] subsite. The resulting pK_a is consistent with the observed acidic optimum pH of activity (Table S5, Figure 6E).

PLs Binding GlcA at the [+1] Subsite Displaying $(\alpha/\alpha)_n$ Barrel Fold. Smlt1473 is the first biochemically and structurally characterized pH-directed multifunctional PL that displays $(\alpha/\alpha)_n$ barrel fold and optimally cleaves HA at pH 5.0. This pH optimum is similar to its PL-8 counterparts, which also utilize a His/Tyr catalytic system. However, the His/Tyr system in Smlt1473 lies in the *anti*-position in comparison to the *syn*-position of PL-8. Thus, there is a possibility of more than one catalytic base candidate based on catalytic geometry.[1] The catalytic base candidates include R215 interacting with the carboxylic group at the [+1] subsite, H168 that also interacts with the carboxylic group and other polar atom in the sugar ring at the [+1] subsite, and Y222 that is in position to act as both catalytic base and acid.[1] We subjected the HA docked Smlt1473 structure to pK_a calculation to analyze the above possibilities.

In the apo state, H168 pK_a is well below 5 due to its lack of solvent accessibility and Coulombic interaction with only pK_a lowering basic amino acid R215 at the [+1] subsite (Table S6). In contrast, R215 has a pK_a value greater than its intrinsic pK_a value due to pK_a raising H-bond interaction from Y222 at the [+1] subsite and Coulombic interaction from Y39, Y115, and Y222 at the [+1] subsite and Y38 and Y225 at the [−1] subsite. Additionally, the Coulombic interaction from the acidic amino acids such as E212 at the [+1] subsite and D41 at the [+2] subsite further raises the pK_a (Table S6). For Y222, the pK_a raising Coulombic interaction from D41, Y38, Y39, Y115, Y225, and E212 at subsites overwhelms the pK_a lowering H-bond interaction from R215 and Coulombic interaction from R215 and R218 (Table S6). In the bound state, the increase in H168 pK_a is consistent with the acidic optimum pH of activity. The pK_a increasing interaction includes H-bond interaction with glycosidic oxygen atom between the [+2] and [+1] sugar unit and sugar ring oxygen atom at the [+1] subsite. The Coulombic interaction from the substrate carboxylic group at the [+1] subsite and D111 at the [+2] subsite further contributes to the rise in H168 pK_a (Table S6). For R215, there are no pK_a lowering interactions, so its pK_a is much higher; therefore, it is unable to act as catalytic base (Table S6). Similarly, Y222 is also substantially altered with pK_a raising determinants, thus also precluding it from acting as base at acidic pH (Table S6, Figure 6F). The amino acid residue H168 has a pK_a consistent to act as base; however, its *anti*-position with respect to labile C5-H at the [+1] subsite precludes such a possibility. The other residues that are in the *syn*-position to labile C5-H have very high pK_a values. Thus, a more comprehensive analyses based on QM/MM methods may be required to fully elucidate this mechanism.

PLs Binding IdoA at the [+1] Subsite Displaying β-Jellyroll Fold. Heparinase-I is the only biochemically and structurally characterized PL that cleaves the most negatively charged glycan (heparin sulfate). It utilizes a His/Tyr system as discussed above

https://doi.org/10.1021/acs.biochem.3c00321
Biochemistry XXXX, XXX, XXX−XXX

for poly-GlcA cleaving PLs. In particular, the heparinase-I His/Tyr system is more similar to Smlt1473; however, in contrast to Smlt1473, the IdoA substrate's labile C5-H at the [+1] subsite is in *syn*-position with respect to H151, clearly establishing H151 as the catalytic base. In the apo state, H151 has a very low pK_a due to no solvent accessibility and availability of only pK_a lowering determinants that include R83, K353 at the [+2, +1] subsite, and R344 at the [−1] subsite (Table S7). In the bound state, H151 pK_a increases in comparison to the apo state because of interaction mainly from the substrate that includes H-bond interactions from glycosidic oxygen atom between the [+2] and the [+1] subsite, ring oxygen atom at the [+1] subsite, and main chain oxygen atom of G152 at the [+1] subsite. The pK_a raising Coulombic interactions include contribution from carboxylic groups at the [+3] and [+1] subsite, whereas the pK_a lowering Coulombic interactions include K81 and K252 at the [+1] subsite, R344 at the [+1, −1] subsite, and R83 and K353 and interaction with the substrate N-group bonded with the SO_4 group at the [+2] and [−1] subsite. The binding of highly negatively charged substrate does not raise the pK_a significantly because of predominant pK_a lowering interaction and no solvent accessibility (Table S7, Figure 6G).

PLs Binding GlcA at the [+1] Subsite Displaying β-Propeller Fold. Ulvan is a sulfated, nonglycan anionic polysaccharide that contains a GlcA group bound by PLs at the [+1] subsite. LOR_107 is a biochemically and structurally characterized ulvan lyase that cleaves glycosidic bond between GlcA and RG[3S]. H146 is thought to act as both the base and acid due to its spatial position with respect to the bound substrate at the [+1] subsite, whereas R259 acts as a charge neutralizer. This is the first instance among PLs where His is acting as base as well as acid.[18] In the apo state, H146 forms two pK_a lowering Coulombic interactions with H167 and R259 at the [+1] subsite. The pK_a raising interactions include H-bond and Coulombic interaction from E144 at the [+1] subsite. Despite the higher contribution from the negatively charged interactions, the low solvent accessibility adds the pK_a lowering determinants to decrease the pK_a one unit below their intrinsic value (Table S7). In the bound state, the pK_a lowering determinants for H146 are preserved as apo states, H167, and R259. Apart from the pK_a raising H-bond and Coulombic interaction from E144, the other pK_a raising contributions from the substrate include H-bond interactions from cleavable glycosidic bond oxygen atom at the [−1, +1] subsite, ring oxygen atom at the [+1] subsite, and the Coulombic interaction from the carboxylic group at the [+1] subsite. Similar to apo state, the lack of solvent accessibility of the catalytic base overwhelms the pK_a raising negatively charged interaction to maintain similar pK_a as the apo state (Table S7, Figure 6H).

PLs Binding ManA at the [+1] Subsite Displaying $(\alpha/\alpha)_n$ Barrel Fold. The PL-5 family of PLs is biochemically and structurally well characterized for cleaving ManA at optimum alkaline pH values. The selected PL-5 enzymes for pK_a analysis include alginate lyase A1-III and Smlt1473; the catalytic system utilized by these PLs is similar to heparinase-I as discussed above. However, the alginate lyase A1-III and Smlt1473 have structurally more than one choice for catalytic base residue due to their catalytic geometry. These residues include H192, R239, and Y246 for alginate lyase A1-III and structurally conserved H168, R215, and Y222 for Smlt1473. We analyzed each of these amino acid residues for their ability to act as the catalytic base.

For alginate lyase A1-III, the H192 in apo state interacts with pK_a lowering R196 and R239 occupying the [+2] and [+1] subsite, respectively. The pK_a raising determinants include H-bond interaction with E140 and Coulombic interaction with E140 and E236 at the [+1] subsite. A very low H192 solvent accessibility balances the predominant negatively charged interaction, resulting in pK_a rising slightly above its intrinsic value (Table S8). In the bound state, H192 maintains the same pK_a lowering residues as apo state: R196 and R239. The pK_a raising interactions are also maintained as apo state: E140 and E236. However, the additional pK_a raising contribution from bound substrate (sugar ring oxygen and carboxylic group) at the [+1] subsite negates the pK_a lowering effect of H192's lack of solvent accessibility. Interestingly, the pK_a increases to values consistent with the optimum pH of activity (Table S8). For R239 in apo state, there are only weak but pK_a raising determinants at the [+1] subsite that include H-bond interaction with Y246 and Coulombic interaction involving Y137, Y246, E236, and E241 at the [+1] subsite. The high solvent accessibility of R239 balances the contribution of pK_a lowering interactions resulting in intrinsic pK_a values (Table S8). In the bound state, R239 interacts weakly with pK_a lowering R67 at the [−1] subsite. The pK_a raising interactions from apo state are preserved except for new contributions from Y68 and the substrate carboxylic group at the [+1] subsite. The pK_a raising interactions in the bound state overwhelm the pK_a lowering effect of R239 low solvent accessibility, precluding its possibility as catalytic base and thus limiting its use as an aide only in charge neutralization and substrate stabilization (Table S8). For Y246 in apo state, the pK_a lowering determinants include H-bond and Coulombic interaction from R239 at [+1] and Coulombic interaction from R306 at the [−2] subsite. The pK_a raising contribution in the form of Coulombic interactions include E236 and E241 at the [+1] subsite and D304 and D314 at the [−2] subsite (Table S8). For Y246 in bound state, the pK_a lowering interactions from R239 and R306 are preserved but include additional contribution from H-bond interactions from substrate glycosidic oxygen at the [+1, −1] subsite and hydroxyl group oxygen R67 at the [−1] subsite. The pK_a raising contributions from negatively charged residues in apo state are preserved except D314. The new contributions include H-bond and Coulombic interactions from Y68 and Coulombic interaction from Y80 at the [−1] subsite with a strong, moderate, and almost negligible Coulombic interaction from substrate carboxylic groups at [+1], [−1], and [−2] subsites, respectively. The lack of solvent accessibility of Y246 heavily aids the pK_a raising contribution from negatively charged residues, and thus, pK_a jumps well above the intrinsic values (Table S8, Figure 7A).

This present situation is similar to what we observed above for pK_a analysis of Smlt1473 docked with HA, the only residue consistently acting as catalytic base (H168) at the observed optimum pH of activity, which structurally is similar to the conserved His (H192) residue in alginate lyase A1-III. However, its *anti*-orientation[1,7−9] with the substrate's labile C5-H group at the [+1] subsite geometrically precludes its ability to act as catalytic base.

For pK_a analysis of ManA-bound Smlt1473, we modeled the sugar unit at the [−3] subsite as it is not modeled in the deposited crystal structure. In the bound state, H168 has one pK_a lowering determinant: R215 at the [+1] subsite. In contrast, the pK_a raising determinants include H-bond interaction with sugar ring oxygen at the [+1] subsite. The other pK_a raising determinant includes D111 and carboxylic group at the [+2] and

https://doi.org/10.1021/acs.biochem.3c00321
Biochemistry XXXX, XXX, XXX−XXX

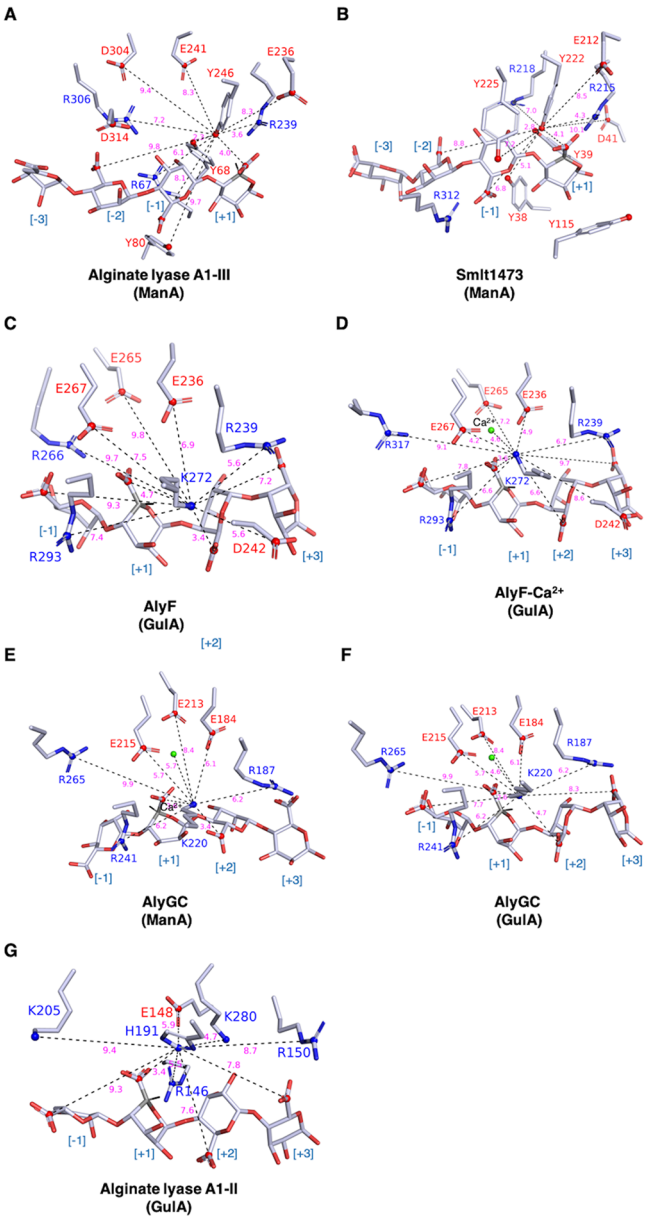

Figure 7. Electrostatic microenvironment around catalytic base of selected poly-ManA/GulA lyases. (A) Alginate lyase A1-III complexed with tetra-ManA [−3 to +1], catalytic base: Y246 [+1]; (B) Smlt1473 complexed with tetra-ManA [−3 to +1], catalytic base: Y222 [+1]; (C) AlyF complexed with tetra-GulA [−1 to +3], catalytic base: K272 [+1]; (D) AlyF complexed with Ca^{2+} (modeled) and tetra-GulA [−1 to +3], catalytic base: K272 [+1]; (E) AlyGC complexed with Ca^{2+} and tetra-ManA [−1 to +3], catalytic base: K220; (F) AlyGC complexed (modeled) with Ca^{2+} and tetra-GulA [−1 to +3], catalytic base: K220; and (G) alginate lyase A1-II complexed with tetra-GulA [−1 to +3], catalytic base: H191 [+1]. The figure coloring and styling are the same as Figure 5 (see figure legends).

[+1] subsites, respectively. The lack of solvent accessibility for H168 lowers the pK_a well below the intrinsic values (Table S8).

For R215 in the bound state, there is the presence of only pK_a raising interactions that include H-bond and Coulombic interaction with carboxylic group at the [+1] subsite and Y222 at the [+1, −1] subsite. The other pK_a raising determinants include D41(93) at the [+2] subsite; Y39(27), Y115(17), and E212(0) at the [+1] subsite; and Y38 and Y225 at the [−1] subsite. The presence of only negatively charged interactions balances the pK_a lowering effect for R215 due to low solvent accessibility, thus rendering it to function only as a substrate stabilizer (Table S8). For Y222, the pK_a lowering determinants include H-bond interaction with glycosidic oxygen at the [+1, −1] subsite, C2-hydroxyl group at the [−1] subsite, and R215 at the [+1] subsite. The pK_a lowering Coulombic interactions are from side chains of R215 and R218. The pK_a raising determinants include H-bond interaction from Y39 and Coulombic interaction with D41, E212, Y38, Y39, Y225, and carboxylic groups at [+1, −1, −2] subsites (Table S8, Figure 7B).

The lack of solvent accessibility coupled with overwhelming interactions from negatively charged determinants from protein and substrates significantly raises Y222 pK_a to act as the catalytic base (Table S8). Interestingly, only H168 has a suitable electrostatic environment for functioning as catalytic base, but its *anti*-orientation with respect to labile substrate C5-H at the [+1] subsite geometrically precludes that from happening. In previous studies, it has been confirmed that Smlt1473 can cleave poly-GulA (C5 epimer of ManA),[2,3] which contains labile substrate C5-H in *syn*-orientation with respect to H168. However, Smlt1473 activity toward poly-GulA is low, suggesting an elusive catalytic mechanism not yet captured by current structural and computational analysis. In subsequent sections, we end this structural−computational analyses with discussion of PLs binding GulA at the [+1] subsite, where we will encounter PL-6 with parallel β-helix fold that is structurally and catalytically similar to poly-GalA lyase discussed in the previous section. We will also encounter the PL-7 family of poly-GulA lyase utilizing a His/Tyr system similar to PL-5 but embedded in a β-sandwich fold.

PLs Binding GulA at the [+1] Subsite Displaying Parallel β-helix Fold. The PL-6 family of PLs is known to cleave alginates and chondroitin sulfates, and like their structural homolog poly-GalA lyase, they utilize metal ion (Ca^{2+}) for charge neutralization. The only biochemically and structurally well-characterized (apo and substrate bound) PL-6 members are poly-GulA specific lyases AlyF and AlyGC; hence, we selected these two PLs for structural and computational analyses. It has been reported for AlyF that it does not require the presence of Ca^{2+} ion for its enzyme catalysis.[33] However, it does contain the Ca^{2+} ion binding site like other PL-6 (e.g., AlyGC), so we added the Ca^{2+} ion at the identified binding site in the substrate bound structure (AlyF-Ca^{2+}) and relaxed it before pK_a analysis. First, we will discuss the result of AlyF's pK_a analysis without bound Ca^{2+} as reported in the literature.[33] In apo state, K272's pK_a lowering determinants include R239 at the [+3] subsite and R266 and R293 at the [−1] subsite. The pK_a raising determinants include D242 at the [+3] subsite and E265, E236, and E267 at the [+1] subsite. The higher contribution of negatively charged pK_a raising determinants is balanced largely by the lack of solvent accessibility of K272; thus, pK_a decreases only by a unit below the intrinsic value. The protein coordinate in apo state does not contain the Ca^{2+} ion at the [+1] subsite; otherwise, we would have captured lower pK_a values (Table S9). In bound state, the pK_a lowering determinants are preserved as apo state and have the same low solvent accessibility. The pK_a raising determinants apart from D242, E265, E236, and E267 include H-bond and Coulombic interaction from carboxylic group at the [+2] subsite and other Coulombic interaction from carboxylic groups at [+3], [+1], and [−1] subsites. Interestingly, the pK_a values of all pK_a raising determinants, except the substrate carboxylic group and D242, are much higher than their

https://doi.org/10.1021/acs.biochem.3c00321
Biochemistry XXXX, XXX, XXX−XXX

intrinsic values and lie in near-neutral to alkaline pH range (E265, E236, and E267). Because of their high pK_a (near optimum pH), if we neglect the contribution of the pK_a raising determinants, the pK_a of the K272 in the bound state will be similar to apo AlyF (Table S9, Figure 7C). We will next discuss the result of pK_a analysis of substrate bound AlyF modeled with Ca^{2+} ion at the [+1] subsite (AlyF-Ca^{2+}), as it may shed light on why AlyF may not require Ca^{2+} for its functioning. In AlyF-Ca^{2+}, the K272 pK_a lowering determinants apart from R239 and R293 include R317 at the [−1] subsite. The R317 replaces the role of nearby R266 observed in AlyF substrate bound. The pK_a raising determinants are the same as AlyF-Ca^{2+}, but in contrast to AlyF, the pK_a of residue E265 is in the alkaline range. The lowering of pK_a for other residues such as E236 and E267 can be attributed to the bound Ca^{2+} ion, as its presence has repacked the side chain of E236 and E267 in such a way that they experience less pK_a raising negative charge interactions in comparison to those of substrate bound AlyF. This suggests that the presence of Ca^{2+} ion lowers the pK_a of acidic amino acid clusters at the [+1] subsite. The low pK_a of these amino acids will make them negatively charged at low pH, and the resulting negative charge interactions will raise the catalytic base (K272) pK_a. The Ca^{2+} ion presence should lower the catalytic base pK_a. However, the overwhelming negative charge from the substrate carboxylic group and acidic amino acid clusters at the [+1] subsite will prevent the lowering of K272's pK_a (Table S9, Figure 7D).

Next, we performed the pK_a calculation for AlyGC that is known to utilize Ca^{2+} ion for catalysis, and we compared it with the AlyF's active site pK_a determinants to understand the differences in the catalytic mechanism. For AlyGC's catalytic base K220 in apo state, the pK_a lowering determinants apart from its low solvent accessibility include positively charged Coulombic interaction from bound Ca^{2+} ion at the [+1] subsite, R187 at the [+3] subsite, and R241 at the [+1, −1] subsite. The pK_a raising determinants include negatively charged Coulombic interactions from E184 at the [+2] subsite and E213 and E215 at the [+1] subsite. The number of pK_a lowering as well as raising interactions with catalytic base (K220) is less compared to the AlyF apo structure (Table S9). The GulA bound state of AlyGC (AlyGC-GulA) was obtained by modeling the GulA (taken from AlyF: PDB ID 6A40) into AlyGC and relaxing the complex using Rosetta. The pK_a lowering interaction for K220 apart from Ca^{2+}, R187, and R241 includes weakly interacting R265 at the [−1] subsite. In comparison to apo state, the AlyGC-GulA's pK_a raising determinants apart from E184, E213, and E215 include H-bond and Coulombic interactions from the carboxylic group at [+1] and [+3, +2] subsites. The carboxylic group interactions are less in comparison to the AlyF substrate bound structure (Table S9, Figure 7F). The ManA bound crystal structure also has the same number of pK_a lowering and raising determinants except for the substrate carboxylic group. The lack of carboxylic group contribution can be attributed to ManA's substrate pose in contrast to its C5-epimer GulA (Table S9, Figure 7E). Recently, the PLs from this family (PL-6) have also been implicated in the cleavage of ManA containing substrate.[34] However, the catalytic Lys is in the opposite direction of ManA's C-5 orientation at the [+1] subsite, suggesting a highly dynamic binding site like PL-5.

PLs Binding GulA at the [+1] Subsite Displaying β-Sandwich Fold. The PL-7 family of PLs is known to specifically bind and cleave poly-GulA. Unlike the PL-6's Lys/Arg catalytic system, the alginate lyase from PL-7 utilizes the His/Tyr system similar to PL-5. Alginate lyase A1-II is one such structurally and biochemically characterized PL that we have selected for the pK_a analyses. The catalytic base H191 interacts predominantly with pK_a lowering amino acids R150 at the [+3] subsite, K280 at the [+2] subsite, R146 at the [+1] subsite, and K205 at the [−1] subsite. The pK_a raising determinants include the backbone H-bond interaction from G192 at the [+1] subsite and Coulombic interaction from E148 at the [+1] subsite (Table S9). In the bound state, the pK_a lowering determinants are the same as in the apo state: R146, R150, K280, and K205. Meanwhile, the pK_a raising contributions include the Coulombic interaction from E148 and carboxylic groups at [+3, +2, +1, −1] subsites. The increase in negative charge contributions from the substrate carboxylic group raises the pK_a of substrate bound alginate lyase A1-II's H191 in contrast to apo state (Table S9, Figure 7G).

CONCLUSIONS

The unique ability of Smlt1473 to cleave multiple substrates as a function of pH inspired the preliminary analyses and compiling of data in light of the PL−pH functional relationship (Table 1). The finding that monospecific PLs utilize similar pH as Smlt1473 does for each of its multiple substrates extended our search for all major substrates and focused it explicitly on substrate−pH pairing (Figure 2−4). Interestingly, huge structural differences among PLs did not deter the catalytic pH range for the same substrates. The PLs among each substrate group (Figure 1, Figure S1) and members within and among families were structurally and sequentially compared to account for similarities and differences. For PLs with closely related structures, both sequence and structural alignments were performed. We also found that substrate-coordinate-based structural alignment is more informative. It can be used to find structural convergence at active sites among PLs, which fundamentally vary at the fold level (Figures S4−S14). The result of PLs subjected to pK_a analysis was based not only on numerical values that set very close arguments with the observed working pH of PLs but also on the Coulombic and other noncovalent interaction network (which influences numerical values) modeled in stick representation (Figures 5−7). Overall, this study aims to provide a knowledge base to inspire the development of future bioengineering research involving PLs or other enzymes where pH plays a significant role in substrate binding or cleavage. However, further analyses of change in charged surfaces area [electropositive (low pH) → electronegative (high pH)] among PLs by modeling proteinwide Coulombic interaction network and electrostatic map at different pHs (including optimum pH as the center) will generate further information that can be used to identify regions distal to the active site for controlling and modeling new native or non-native functions.

ASSOCIATED CONTENT

Supporting Information

The Supporting Information is available free of charge at https://pubs.acs.org/doi/10.1021/acs.biochem.3c00321.

Additional methods on calculation of pK_a values and summary of enzymes available including structural and functional data used in analysis and representative structures from enzyme families analyzed in complex with substrates (PDF)

https://doi.org/10.1021/acs.biochem.3c00321
Biochemistry XXXX, XXX, XXX−XXX

AUTHOR INFORMATION

Corresponding Authors

Bryan W. Berger − *Department of Chemical Engineering, University of Virginia, Charlottesville, Virginia 22904, United States;* orcid.org/0000-0002-6135-8677; Email: bryan.berger@virginia.edu

Rudresh Acharya − *School of Biological Sciences, National Institute of Science Education and Research, Bhubaneswar 752050 Odisha, India; Homi Bhabha National Institute, Mumbai 400094 Maharashtra, India;* orcid.org/0000-0002-9012-9849; Email: rudresh.acharya@niser.ac.in

Author

Shubhant Pandey − *School of Biological Sciences, National Institute of Science Education and Research, Bhubaneswar 752050 Odisha, India; Homi Bhabha National Institute, Mumbai 400094 Maharashtra, India;* orcid.org/0000-0003-3153-8949

Complete contact information is available at: https://pubs.acs.org/10.1021/acs.biochem.3c00321

Author Contributions

S.P.: Conceptualization, Methodology, Data curation, Software, Formal analysis, Validation, Writing − original draft, Writing − review & editing. B.W.B.: Funding acquisition, Investigation, Writing − review & editing, Supervision. R.A.: Conceptualization, Methodology, Formal analysis, Supervision, Funding acquisition, Investigation, Project administration, Writing − original draft, Writing − review & editing, Resources.

Notes

The authors declare no competing financial interest.

All authors have seen and approved the manuscript, and it has not been accepted or published elsewhere.

ACKNOWLEDGMENTS

S.P. and R.A.: We thank NISER for funding. This work was supported in part by the Department of Biotechnology, Govt. of India, grant BT/PR15324/BRB/10/1482/2016. B.W.B.: This work was supported in part by a grant from the Center for Innovative Technology, a Research Innovation Award from the University of Virginia School of Engineering and Applied Science, and a grant from the National Science Foundation (CBET 2211060).

REFERENCES

(1) Pandey, S.; Mahanta, P.; Berger, B. W.; Acharya, R. Structural insights into the mechanism of pH-selective substrate specificity of the polysaccharide lyase Smlt1473. *J. Biol. Chem.* **2021**, *297*, No. 101014.

(2) MacDonald, L. C.; Berger, B. W. A polysaccharide lyase from Stenotrophomonas maltophilia with a unique, pH-regulated substrate specificity. *J. Biol. Chem.* **2014**, *289*, 312−325.

(3) Macdonald, L. C.; Berger, B. W. Insight into the role of substrate-binding residues in conferring substrate specificity for the multifunctional polysaccharide lyase Smlt1473. *J. Biol. Chem.* **2014**, *289*, 18022−18032.

(4) Li, S.; Kelly, S. J.; Lamani, E.; Ferraroni, M.; Jedrzejas, M. J. Structural basis of hyaluronan degradation by Streptococcus pneumoniae hyaluronate lyase. *EMBO J.* **2000**, *19*, 1228−1240.

(5) Jedrzejas, M. J.; Mello, L. V.; De Groot, B. L.; Li, S. Mechanism of hyaluronan degradation by Streptococcus pneumoniae hyaluronate lyase. Structures of complexes with the substrate. *J. Biol. Chem.* **2002**, *277*, 28287−28297.

(6) Elmabrouk, Z. H.; Vincent, F.; Zhang, M.; Smith, N. L.; Turkenburg, J. P.; Charnock, S. J.; Black, G. W.; Taylor, E. J. Crystal structures of a family 8 polysaccharide lyase reveal open and highly occluded substrate-binding cleft conformations. *Proteins: Struct., Funct., Bioinf.* **2011**, *79*, 965−974.

(7) Yoon, H. J.; Mikami, B.; Hashimoto, W.; Murata, K. Crystal structure of alginate lyase A1-III from Sphingomonas species A1 at 1.78 Å resolution. *J. Mol. Biol.* **1999**, *290*, 505−514.

(8) Yoon, H. J.; Hashimoto, W.; Miyake, O.; Murata, K.; Mikami, B. Crystal structure of alginate lyase A1-III complexed with trisaccharide product at 2.0 Å resolution. *J. Mol. Biol.* **2001**, *307*, 9−16.

(9) Mikami, B.; Ban, M.; Suzuki, S.; Yoon, H. J.; Miyake, O.; Yamasaki, M.; Ogura, K.; Maruyama, Y.; Hashimoto, W.; Murata, K. Induced-fit motion of a lid loop involved in catalysis in alginate lyase A1-III. *Acta Crystallogr., Sect. D: Biol. Crystallogr.* **2012**, *68*, 1207−1216.

(10) Dash, P.; Acharya, R. Distinct Modes of Hidden Structural Dynamics in the Functioning of an Allosteric Polysaccharide Lyase. *ACS Cent. Sci.* **2022**, *8*, 933−947.

(11) Garron, M. L.; Cygler, M. Structural and mechanistic classification of uronic acid-containing polysaccharide lyases. *Glycobiology* **2010**, *20*, 1547−1573.

(12) Féthière, J.; Eggimann, B.; Cygler, M. Crystal structure of chondroitin AC lyase, a representative of a family of glycosaminoglycan degrading enzymes. *J. Mol. Biol.* **1999**, *288*, 635−647.

(13) Huang, W.; Boju, L.; Tkalec, L.; Su, H.; Yang, H.-O.; Gunay, N. S.; Linhardt, R. J.; Kim, Y. S.; Matte, A.; Cygler, M. Active site of chondroitin AC lyase revealed by the structure of enzyme - Oligosaccharide complexes and mutagenesis. *Biochemistry* **2001**, *40*, 2359−2372.

(14) Lunin, V. V.; Li, Y.; Linhardt, R. J.; Miyazono, H.; Kyogashima, M.; Kaneko, T.; Bell, A. W.; Cygler, M. High-resolution crystal structure of Arthrobacter aurescens chondroitin AC lyase: An enzyme-substrate complex defines the catalytic mechanism. *J. Mol. Biol.* **2004**, *337*, 367−386.

(15) Huang, W.; Matte, A.; Li, Y.; Kim, Y. S.; Linhardt, R. J.; Su, H.; Cygler, M. Crystal structure of chondroitinase B from Flavobacterium heparinumand its complex with a disaccharide product at 1.7 Å resolution. *J. Mol. Biol.* **1999**, *294*, 1257−1269.

(16) Michel, G.; Pojasek, K.; Li, Y.; Sulea, T.; Linhardt, R. J.; Raman, R.; Prabhakar, V.; Sasisekharan, R.; Cygler, M. The Structure of Chondroitin B Lyase Complexed with Glycosaminoglycan Oligosaccharides Unravels a Calcium-dependent Catalytic Machinery. *J. Biol. Chem.* **2004**, *279*, 32882−32896.

(17) Han, Y. H.; Garron, M. L.; Kim, H. Y.; Kim, W. S.; Zhang, Z.; Ryu, K. S.; Shaya, D.; Xiao, Z.; Cheong, C.; Kim, Y. S.; Linhardt, R. J.; Jeon, Y. H.; Cygler, M. Structural snapshots of heparin depolymerization by heparin lyase I. *J. Biol. Chem.* **2009**, *284*, 34019−34027.

(18) Ulaganathan, T.; Helbert, W.; Kopel, M.; Banin, E.; Cygler, M. Structure-function analyses of a PL24 family ulvan lyase reveal key features and suggest its catalytic mechanism. *J. Biol. Chem.* **2018**, *293*, 4026−4036.

(19) Yamasaki, M.; Ogura, K.; Hashimoto, W.; Mikami, B.; Murata, K. A structural basis for depolymerization of alginate by polysaccharide lyase family-7. *J. Mol. Biol.* **2005**, *352*, 11−21.

(20) Alford, R. F.; Leaver-Fay, A.; Jeliazkov, J. R.; O'Meara, M. J.; DiMaio, F. P.; Park, H.; Shapovalov, M. V.; Renfrew, P. D.; Mulligan, V. K.; Kappel, K.; Labonte, J. W.; Pacella, M. S.; Bonneau, R.; Bradley, P.; Dunbrack, R. L., Jr.; Das, R.; Baker, D.; Kuhlman, B.; Kortemme, T.; Gray, J. J. The Rosetta All-Atom Energy Function for Macromolecular Modeling and Design. *J. Chem. Theory Comput.* **2022**, *18*, 4594.

(21) Søndergaard, C. R.; Olsson, M. H. M.; Rostkowski, M.; Jensen, J. H. Improved treatment of ligands and coupling effects in empirical calculation and rationalization of pKa values. *J. Chem. Theory Comput.* **2011**, *7*, 2284−2295.

(22) Olsson, M. H. M.; Søndergaard, C. R.; Rostkowski, M.; Jensen, J. H. PROPKA3: Consistent treatment of internal and surface residues in empirical pKa predictions. *J. Chem. Theory Comput.* **2011**, *7*, 525−537.

(23) Bezençon, J.; Wittwer, M. B.; Cutting, B.; Smieško, M.; Wagner, B.; Kansy, M.; Ernst, B. pKa determination by 1H NMR spectroscopy − An old methodology revisited. *J. Pharm. Biomed. Anal.* **2014**, *93*, 147−155.

(24) Pace, C. N.; Grimsley, G. R.; Scholtz, J. M. Protein ionizable groups: pK values and their contribution to protein stability and solubility. *J. Biol. Chem.* **2009**, *284*, 13285−13289.
(25) Alahuhta, M.; Taylor, L. E.; Brunecky, R.; Sammond, D. W.; Michener, W.; Adams, M. W. W.; Himmel, M. E.; Bomble, Y. J.; Lunin, V. The catalytic mechanism and unique low pH optimum of Caldicellulosiruptor bescii family 3 pectate lyase. *Acta Crystallogr., Sect. D: Biol. Crystallogr.* **2015**, *71*, 1946−1954.
(26) Luis, A. S.; Briggs, J.; Zhang, X.; Farnell, B.; Ndeh, D.; Labourel, A.; et al. Dietary pectic glycans are degraded by coordinated enzyme pathways in human colonic Bacteroides. *Nat. Microbiol.* **2018**, *3*, 210−219.
(27) Scavetta, R. D.; Herron, S. R.; Hotchkiss, A. T.; Kita, N.; Keen, N. T.; Benen, J. A. E.; et al. Structure of a plant cell wall fragment complexed to pectate lyase C. *Plant Cell* **1999**, *11*, 1081−1092.
(28) Herron, S. R.; Scavetta, R. D.; Garrett, M.; Legner, M.; Jurnak, F. Characterization and implications of Ca2+ binding to pectate lyase C. *J. Biol. Chem.* **2003**, *278*, 12271−12277.
(29) Zheng, Y.; Huang, C. H.; Liu, W.; Ko, T. P.; Xue, Y.; Zhou, C.; Guo, R. T.; Ma, Y. Crystal structure and substrate-binding mode of a novel pectate lyase from alkaliphilic Bacillus sp. N16-5. *Biochem. Biophys. Res. Commun.* **2012**, *420*, 269−274.
(30) Seyedarabi, A.; To, T. T.; Ali, S.; Hussain, S.; Fries, M.; Madsen, R.; Clausen, M. H.; Teixteira, S.; Brocklehurst, K.; Pickersgill, R. W. Structural insights into substrate specificity and the anti β-elimination mechanism of pectate lyase. *Biochemistry* **2010**, *49*, 539−546.
(31) Abbott, D. W.; Boraston, A. B. A family 2 pectate lyase displays a rare fold and transition metal-assisted β-elimination. *J. Biol. Chem.* **2007**, *282*, 35328−35336.
(32) Charnock, S. J.; Brown, I. E.; Turkenburg, J. P.; Black, G. W.; Davies, G. J. Convergent evolution sheds light on the anti-β-elimination mechanism common to family 1 and 10 polysaccharide lyases. *Proc. Natl. Acad. Sci. U. S. A.* **2002**, *99*, 12067−12072.
(33) Lyu, Q.; Zhang, K.; Shi, Y.; Li, W.; Diao, X.; Liu, W. Structural insights into a novel Ca^{2+}-independent PL-6 alginate lyase from Vibrio OU02 identify the possible subsites responsible for product distribution. *Biochim. Biophys. Acta, Gen. Subj.* **2019**, *1863*, 1167−1176.
(34) Violot, S.; Galisson, F.; Carrique, L.; Jugnarain, V.; Conchou, L.; Robert, X.; Thureau, A.; Helbert, W.; Aghajari, N.; Ballut, L. Exploring molecular determinants of polysaccharide lyase family 6−1 enzyme activity. *Glycobiology* **2021**, *31*, 1557−1570.

https://doi.org/10.1021/acs.biochem.3c00321
Biochemistry XXXX, XXX, XXX−XXX